

## **Chapter VII**

### **Summary and Conclusions**

#### **7.1. Introduction**

The progress of mankind has always intimately related to the availability of “Energy”. The energy needs of a society for its sustenance are increasing at a faster rate since its existence. Earlier the needs were in the form of food. With the passage of time man began to use the fire, wind and water for his energy demands. He started cultivating land for agriculture and training animals to work for him and thus gave a new dimension to the use of energy. At that time Sun was fulfilling all the energy needs of a mankind either directly or indirectly. A turning point was the discovery of steam engine (AD 1700), which has initiated the Industrial Revolution and man began to use new sources of energy, viz. fossil fuels in large quantities. The fossil fuels era then (non-renewable sources) began and energy is now available in a concentrated form. Nuclear energy came on the scene after the II World War that provided a significant but a very small range of the energy requirements of the many countries. Today every country draws its energy needs from a variety of sources which can be broadly classified as commercial and non-commercial. The commercial sources include the fossil fuels (coal, oil and natural gas), hydro-electric power and nuclear power, while the non-commercial sources include wood, animal wastes and agricultural wastes. In the industrialized countries, most of the energy needs are met from commercial sources, while developing countries like India, the use of commercial and non-commercial sources are being made. In the early 1970s, the disruption of oil supplies to the industrialized world spurred to the

serious consideration of another terrestrial power source. In order to meet the energy requirements of the world population with an average electricity supply of 1 kW/ head, at present, an average of around 100 GW of new capacity would have to be installed each year. For several reasons, neither fossil fuels nor nuclear energy could supply more than a fraction of such a large increase in electricity demand. First of all, these resources are fast depleting and the fossil fuel era is gradually coming to an end, especially oil and natural gases. As well, if fossil fuel were to supply more than a small part of the required capacity, it would cause severe environmental pollution and damages. They may contribute unpredictable and irreversible climate changes in the near future through the emission, mainly of carbon dioxide and carbon monoxide. The use of nuclear energy, on even a fraction of this scale would also have severe environmental consequences and in view of the continuing political and religious conflicts around the World, would seem likely to lead to widespread proliferation of nuclear weapons.

As an alternative, photovoltaic (PV) power generation has gained a considerable momentum. This trend was reinforced by public controversy over nuclear fission reactors and by a series of mishaps in nuclear power stations, especially those of Three Mile Island (in 1979), Chernobyl (in 1986) and Fukushima (in 2011). Since the beginning of the 1990s, ecological considerations linked with the CO<sub>2</sub>/global warming have taken over as a main driving force in promoting PV solar energy. Photovoltaics is the most useful way of utilizing solar energy by directly converting it into electricity. It is the generation of an electromotive force as a result of the absorption of ionizing

radiation. Photovoltaic energy not only can meet the growing worldwide demand for electricity, but it can do so without incurring the high economic and environmental costs of burning fossil fuels and installing power lines. It is the most attractive non-conventional energy source of proven reliability from the micro to the mega-watt level. PV technology needs only a simple solid state device for direct conversion of abundant solar light into electricity at room temperature. Energy conversion devices which are used to convert sun light into electricity by the use of the photovoltaic effect are called solar cells and are pollution free hence eco-friendly. There are no moving parts and if the device is correctly encapsulated against the environment, there is nothing to wear out. These systems are modular and their electrical power output can be engineered, for virtually any application from low-powered consumer uses-wristwatches, calculators and small battery chargers-to energy-significant requirements such as generating power at electric utility central stations. The developing nations with limited conventional power sources, particularly in remote areas, are increasingly turning to PV power for enhancing their development index. Now about 2 GW of solar cells are being used worldwide in a variety of applications, ranging from MW of standalone /grid connected power stations to several MW of low power electronic devices.

Today, in addition to the conventional solar cells, a wide range of solar cell technologies based on a variety of materials such as II-VI, IV-VI, III-V, II- IV-VI, I-III-VI<sub>2</sub>, etc. are being developed and the energy conversion efficiencies in the 5% to 25% range for a single and pure crystals of silicon and cadmium are reported. However, manufacturing

and fabrication costs of silicon based devices put limit on their usage as commercial devices. To overcome these difficulties Semiconductor /Liquid junction approach is gaining much popularity due to its low fabrication cost, high-throughput processing techniques, ease of junction formation and large-scale production over the silicon solar cells. These PV cells based on polycrystalline semiconductor materials provide an economically viable chemical route for trapping the non-pollutant and abundantly scattered solar radiations.

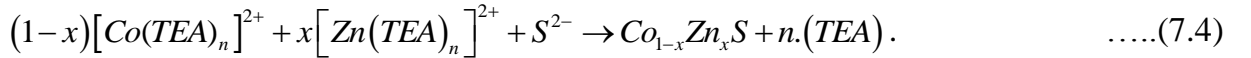
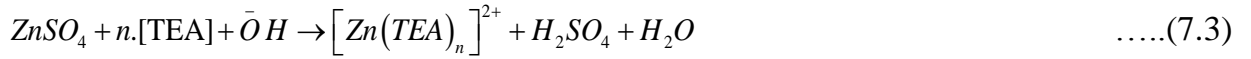
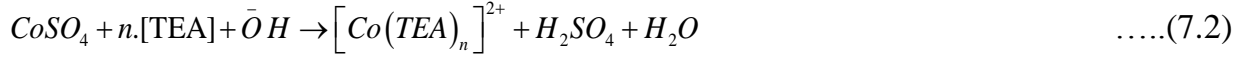
## **7.2. The Synthesis, Reaction Mechanism and Growth Kinetics of CoS and Co<sub>1-x</sub>Zn<sub>x</sub>S Thin Films**

### **7.2.1. The reaction kinetics and growth mechanism**

The Co<sub>1-x</sub>Zn<sub>x</sub>S ( $0 \leq x \leq 0.4$ ) films were deposited from the aqueous solutions of cobalt sulphate, zinc sulphate and thiourea as the precursors. The appropriate volumes of CoSO<sub>4</sub> (1M,10 ml), thiourea (1M,10 ml) and calculated quantity of ZnSO<sub>4</sub> (1M) were taken in a reaction bath and triethanolamine was added to form a complex compound containing Co<sup>2+</sup>, Zn<sup>2+</sup> and S<sup>-2</sup> ions. To this, ammonia was added to enhance the film adherence. The deposition temperature, time, pH of the reaction solution and speed of the substrate rotation were optimized as [1-3];

1. deposition Temperature =  $80 \pm 0.5$  °C
2. deposition Time = 90 min.
3. pH =  $9.0 \pm 0.1$ .
4. speed of the substrate rotation =  $65 \pm 1$  rpm.

The overall reactions can be formulated as [3-5];



Initially, TEA forms a complex with  $Co^{2+}$  and  $Zn^{2+}$ , on the other hand,  $(NH_2)_2CS$  is considered to decompose at a particular temperature to produce  $S^{2-}$  ions. The reaction between  $Co^{2+}/Zn^{2+}$ -TEA complex and  $S^{2-}$  anions originating from the hydrolysis of  $(NH_2)_2CS$  results in the formation of  $Zn(CoS)$  thin film layers.

It has been observed that the quality deposits are obtained with this technique at our experimental conditions [1-4]. The pure CoS samples are dark-sea green in colour whereas colour of the  $Co_{1-x}Zn_xS$  went on ash grey as x was varied from 0 to 0.4. This has indicated the strong possibility of substitution of  $Co^{2+}$  by  $Zn^{2+}$  atoms in the host CoS lattice.

Wettability measurements led to the conclusion that, in our case, CoS and  $Co_{1-x}Zn_xS$  thin films are of hydrophilic in nature as contact angle ( $\theta$ )  $< 90^\circ$ . Typical contact angle measurement showed decrease in the contact angle with the assimilation of Zn in CoS host lattice tending thin films towards hydrophilic behaviour.

### 7.2.2. The compositional and elemental analysis studies

The CoS and  $\text{Co}_{1-x}\text{Zn}_x\text{S}$  ( $0 \leq x \leq 0.4$ ) thin films were then analyzed through the EDS and XPS techniques.

**a) The compositional analysis (EDS)**

The as-grown CoS and  $\text{Co}_{1-x}\text{Zn}_x\text{S}$  ( $0 \leq x \leq 0.4$ ) films were analyzed by an EDS technique. Pure CoS films are rich in  $\text{Co}^{2+}$ . The addition of Zn replaced Co from the CoS lattice whereas,  $\text{S}^{2-}$  content remained almost the same [3, 4]. However, insignificant scattering in the sulfur cannot be denied.

**b) The elemental analysis (XPS)**

The XPS survey spectra were recorded in the BE range from 0 to 1400 eV for six representative samples. Narrow scans for Co, Zn and S were also obtained to give the detailed information about chemical state and elemental percentage in the as-deposited thin films. XPS spectra deconvoluted on Co showed Co  $2p_{3/2}$  and Co  $2p_{1/2}$  energy levels appearing due to the spin-orbital splitting; Co  $2p_{3/2}$  (at  $\sim 780$  eV) and Co  $2p_{1/2}$  (at  $\sim 796$  eV) and shake-up satellites. The observed chemical binding energy shift between Co  $2p_{3/2}$  and Co  $2p_{1/2}$  is comparable with that of pure Co metal which indicates that Co ions are preferred in the +2 oxidation state. In the as-grown  $\text{Co}_{1-x}\text{Zn}_x\text{S}$  thin films, because of the strong spin-orbit coupling, the Zn 2p peak also splits into two; Zn  $2p_{3/2}$  and Zn  $2p_{1/2}$  at 1020.12 eV ( $x=0.05$ ) and 1043.36 eV ( $x=0.05$ ), respectively with a doublet peak energy separation of 23.24 eV. This is in close consonance with the standard separation of 23.1 eV corresponding to  $\text{Zn}^{2+}$  [3, 4]. At higher Zn concentrations in the CoS lattice ( $x = 0.3$ ), the difference in BE's of  $2p_{3/2}$  and  $2p_{1/2}$  is 13.10 eV and this is in excellent

match with the theoretical standard of  $\text{Zn}^{2+}$  [3, 4]. Whereas, narrow scan of S 2p core level indicated the presence of  $\text{S}^{2-}$  chemical state (at 169.5 eV) with a little shift on higher B.E. side. It is further observed the Zn/Co ratio in the film measured by the two techniques is nearly the same.

### **7.3. The Structural and Micro-spectroscopic Analyses of CoS and Zn(CoS) Thin Films**

#### **7.3.1. The structural studies**

The X-ray diffractograms were obtained for these composite films in the  $10^\circ$ –  $80^\circ$   $2\theta$  range with Cu  $K\alpha$  radiation (1.5406 Å). The diffractograms were further analyzed to compute the interplanar distances ( $d$ ), intensities of reflections ( $I/I_{\text{max}}$ ), lattice parameters ( $a$  and  $c$ ) and average crystallite size ( $\bar{D}$ ). Strong and sharp signals indicated well-crystallized hexagonal structure with dominant growth orientation along (101) direction. For this reflection,  $d$  is found to be continuously decreased from 2.691 Å to 2.663 Å for the change of  $x$  from 0 to 0.15, whereas  $I/I_{\text{max}}$  is 100% upto  $x = 0.25$  and thereafter decreased to around 60 % for higher  $x$  values [3, 4]. The existence of two minor reflections, (210) and (511) corresponding to the formation of  $\text{CoS}_2$  and  $\text{Co}_3\text{O}_4$  phases have also been detected. The analysis further showed a noticeable shift in the position of (101) peak; for the composition range  $0 \leq x \leq 0.15$ , it is right shifted, whereas left shift is observed for the  $0.2 \leq x \leq 0.4$  range [3, 4]. Both  $a$  and  $c$  are found to be increased continuously with the integration of Zn into the host CoS. The ratio  $c/a$  is almost constant. Thus continuous changes in the interplanar distance ( $d$ ), lattice parameters ( $a$

and c) and structural similarity suggest that there is a formation of ternary alloy of the type Co-Zn-S over  $0 \leq x \leq 0.15$  composition range [3, 4]. Beyond this composition range, separate phase formation has been detected.

### **7.3.2. The FTIR analysis**

Similar nature of all IR spectra suggested no profound effect of Zn-addition on CoS host. The band around  $946.04 \text{ cm}^{-1}$  ( $x = 0.15$ ) is assigned to the stretching frequency of Zn–O bond which is shifted to  $944.83 \text{ cm}^{-1}$  for ( $x = 0.3$ ) in addition to the increase of band intensity (which is absent for undoped CoS film). The absence and presence of bands in addition to the changing band intensity revealed the substitution of  $\text{Zn}^{2+}$  ions into the CoS lattice. By Zn-doping, it is clearly observed that the characteristic Co–S band near  $1096.88 \text{ cm}^{-1}$  is shifted to the  $\approx 1100 \text{ cm}^{-1}$ . This is a characteristic band for ZnS formation at higher concentration of Zn in CoS [4].

### **7.3.3. The surface topographic studies**

The surface morphologies of the CoS and  $\text{Co}_{1-x}\text{Zn}_x\text{S}$  ( $0 \leq x \leq 0.4$ ) films were therefore viewed through the scanning electron and atomic force microscopes.

#### **a) The scanning electron microscopy**

SEM micrographs for CoS and  $\text{Co}_{1-x}\text{Zn}_x\text{S}$  samples revealed a complex multifaceted webbed morphology with uniform substrate surface coverage. In general, film microstructures consist of a network of elongated crystallites having flake like structure with polygonic shaped vacant spaces between them [1-4]. Inconsequential overgrowth with the formation of a sluggish layer over the entire microstructure and a sort of

recrystallization have also been evidenced for  $x = 0 - 0.075$ . For succeeding compositions ( $x = 0.1$  to  $0.4$ ), micrographs showed clear multifaceted complex network [3, 4]. Further, it is also noted that, with increase in Zn into CoS framework, individual crystallites grow further along with the polygonic voids in between them [1-4].

#### **b) The field emission scanning electron microscopy**

FESEM micrographs of the CoS and  $\text{Co}_{1-x}\text{Zn}_x\text{S}$  samples revealed complex multifaceted webbed network of elongated crystallites resembling like the flakes with uniform substrate surface coverage. The film microstructures consist of a network of elongated crystallites reminiscent of flakes with polygonic shaped vacant spaces between them. Additionally, an overgrowth with the formation of a sluggish layer over the entire microstructure and a sort of recrystallization have also been evidenced for lower concentration of Zn in CoS ( $x = 0$  to  $0.075$ ). For higher compositions ( $x = 0.1$  to  $0.4$ ), micrographs showed clear multifaceted complex network. It is also to be noted that, with increase in Zn into CoS framework, an individual crystallites grow further along with the polygonic voids in between them and a considerable improvement in microstructure has been observed [3, 4].

#### **c) The atomic force microscopy**

Surface topographs ( $10\mu\text{m} \times 10\mu\text{m}$  scan area) of the as-obtained thin films were obtained by an AFM technique. Surface topographs of both CoS and Co-Zn-S thin films consisted of the hillocks and valleys suggesting its crystalline nature [1-4]. The surface topographs revealed improvement of hillocks with the accumulation of Zn into the CoS

matrix, crafting valleys and hence surface tends to be rough. The topographs further showed enhanced crystalline nature with Zn integration and as a result one could see increase in average and RMS roughnesses [3,4]. The increase in RMS roughness can be attributed to the enhanced grain growth as evidenced from the SEM micrographs. For small values of x, film roughness is fairly low with shallow valleys. At moderate levels of Zn addition into CoS structure, roughness also goes on increasing with superficial valleys. As the Zn content in the bath is raised further (x = 0.3 to 0.4), surface becomes rougher and eventually has a cavernous appearance [3, 4].

#### **d) The magnetic force microscopy**

The MFM images for CoS and  $\text{Co}_{1-x}\text{Zn}_x\text{S}$  thin films indicated surface coverage of magnetic clusters mimicking the topographic features. The colour contrast within the aggregates suggests existence of dissimilar magnetic domains [1-4]. In general, the magnetic aggregates exhibit irregular shapes. The differences in colour contrast in these images, suggest the presence of mono and multi-magnetic clusters randomly distributed over the substrate surface area [1-4].

### **7.4. The Optical and Transport Studies of CoS and $\text{Co}_{1-x}\text{Zn}_x\text{S}$ Thin Films**

#### **7.4.1. The optical studies**

The optical transmission spectra of the CoS and  $\text{Co}_{1-x}\text{Zn}_x\text{S}$  thin films were obtained in the range of wavelengths from 200 nm to 1600 nm. The spectra were analyzed to evaluate the absorption coefficient. It is found that the absorption coefficient ( $\alpha$ ) is of the order of  $\approx 10^4 \text{ cm}^{-1} - 10^5 \text{ cm}^{-1}$  for both pure and Zn incorporated samples. A systematic

increase in  $\alpha$  was found with increase in composition parameter upto  $x = 0.3$  due to the creation of localized states within the bandgap. The shift in the absorption edge towards lower wavelength with further increase in Zn content can be explained with the *sp-d* exchange interaction between the band electrons in CoS and localized d electrons of  $\text{Zn}^{2+}$ . The optical gaps were then determined from the  $(\alpha h\nu)^2$  vs.  $h\nu$  variation. It is found that the band gap energy increased from 1.59eV to 2.50 eV with the added Zn-concentration (0 to 0.4). The optical transitions are of the band to band direct type with a transmission index of around 0.5.

#### **7.4.2. The electrical transport studies**

The dark dc electrical conductivities of CoS and  $\text{Co}_{1-x}\text{Zn}_x\text{S}$  samples were measured in the 300 K -550 K temperature range. The temperature dependence of an electrical conductivity showed two distinct conduction mechanisms: a grain boundary scattering limited in the higher temperature region, whereas variable range hopping in the lower temperature range. It is seen that electrical conductivity decreased with  $x$  almost monotonically [4]. This is true up to a value of  $x = 0.1$ . Beyond this value of  $x$  conductivity just saturates. The saturation in the specific conductance at higher concentration of  $\text{Zn}^{2+}$  when it is incorporated in II-VI materials has already been reported [6, 7]. The activation energies of an electrical conduction in both the high and low temperature regions were calculated from the temperature dependence of an electrical conductivity. The thermo power measurements in the 300 K-550 K temperature range showed n-type conduction in these films. The thermo electric power

increased with increase in temperature and this behaviour confirmed that the electrons make the major contribution to the electrical conductivity. From the composition dependence of thermopower, it is seen that the thermoelectric power is increased with the composition parameter (x) increased (0 to 0.2) and then remained almost constant with minor downfall [4]. The carrier densities and mobilities were then calculated and it is observed that, as the composition parameter (x) is increased, the carrier concentration and mobility are found to be decreased. The dependence of carrier mobility on temperature suggests the possibility of scattering mechanism associated with the inter-grain barrier potential. The inter-crystalline barrier potential ( $\Phi_B$ ) increased up to  $x = 0.15$  and then decreased a little. The increase in carrier mobility with temperature prevails the possibility of scattering mechanism associated with the inter-grain barrier potential.

Composition dependence of the spectral sensitivity also showed gradual decrease in photosensitivity upto 0.075 and peaked at  $x = 0.1$  and thereafter decreased. The magnitude of sensitivity is also found to be less.

## **7.5. The CoS and $\text{Co}_{1-x}\text{Zn}_x\text{S}$ Electrode/ Electrolyte Based PV- Studies**

### **7.5.1. The choice of an electrolyte redox couple**

The PV cells were formed with various electrolyte systems and in each case the open circuit photovoltage ( $V_{ph}$ ) and short circuit photocurrent ( $I_{ph}$ ) were measured by changing the electrolyte concentration. It is found that the potassium chloride KCl (0.5

M) electrolyte offers a relatively better match both for CoS and  $\text{Co}_{1-x}\text{Zn}_x\text{S}$  electrode materials.

### **7.5.2. The electrochemical PV cell performance studies**

The electrochemical PV cells were then fabricated using these series of the films as the photoelectrode, potassium chloride (0.5M) as an electrolyte and CoS treated graphite rod as a counter electrode. The mechanism of the charge transfer across the electrode / electrolyte interface was studied through the electrical properties (I-V and C-V in dark, measurement of the built-in-potential ( $\Phi_B$ ), power output characteristics under illumination). The junction ideality factors ( $n_d$ ) were determined for each of the cell and the flat band potentials were determined from the Mott-Schottky plots. Under 25  $\text{mW/cm}^2$  input intensity, power output characteristics were examined and different PV-performance parameters ( $V_{oc}$ ,  $I_{sc}$ ,  $ff\%$ ,  $\eta\%$ ,  $R_s$ ,  $R_{sh}$ , etc.) were determined. From the power output measurements it is seen that  $V_{oc}$  has a maximum value of 404 mV for a cell formed with CoS electrode. For other cells  $V_{oc}$  is decreased with x. The variation in  $V_{oc}$  with composition parameter (x) is not systematic. The variation in short circuit current is also not systematic and the observed variations are due to the light absorption and the cell series resistance ( $R_s$ ) effect. The optical studies on fabricated PV-cells confirmed the manifestation of very large concentration of surface states at the interface causing unsystematic and discouraging status (present) of the material as a PV-material.

## 7.6. Remarks

From the investigations done so far, it has been seen that the structural, micro-spectroscopic, optical and electrical transport properties of the CoS and  $\text{Co}_{1-x}\text{Zn}_x\text{S}$  thin films are strongly dependent on the method of preparation and the film composition (x). The analysis of the electrochemical PV cell properties showed that the PV performance is not encouraging at the present moment. The performance is below the expectation and we attribute this low performance to:

- The low density polycrystalline film morphology which causes high concentration of the lattice and boundary defects.
- The low shunt resistance which is a direct consequence of the microspores present in the films.
- Absence of the post deposition treatments.
- Reflection of the light from the photoelectrode surface.
- The small electron affinity difference between the materials.
- The unsystematic PV-performance may also be attributed to the leakage of photogenerated charge carriers into the electrolyte itself, instead of flowing through the external circuit [8].
- Instead, appropriate window layer and formation of multi junctions are required, provided as devised performance of the material should be improved.

## References

- [1] S.S. Kamble, Andrzej Sikora, S.T. Pawar, N.N. Maldar, L.P. Deshmukh, J. Alloys Compd. 623 (2015) 466.
- [2] S.S. Kamble, A. Sikora, S.T. Pawar, R.C. Kambale, N.N. Maldar, L.P. Deshmukh, J. Alloys Compd. 631 (2015) 303.
- [3] S.S. Kamble, A. Sikora, S.T. Pawar, G.T. Chavan, N.N. Maldar, L.P. Deshmukh, Some Investigations on  $Zn_xCo_{1-x}S$  DMS Thin Films: Chemical Synthesis and Characteristic Properties, 2<sup>nd</sup> International Symposium on Physics and Technology of Sensors (ISPTS-2), 08–10 March, 2015, Pune, India.
- [4] S.S. Kamble, Andrzej Sikora, S.T. Pawar, L.P. Deshmukh, International Conference on Recent Trends and Challenges in Science and Technology (RTCST – 2014), 20 – 22 August, 2014, Pravaranagar, India.
- [5] A.N. Chattarki, N.N. Maldar, L.P. Deshmukh, J. Alloys Compd. 597 (2014) 223.
- [6] L.P. Deshmukh, K.M. Garadkar, D.S. Sutrave. Mater. Chem. Phys. 55 (1998) 30.
- [7] a) M.D. Uplane, S.H. Pawar, Solar Cells 10 (1983) 177.  
b) M.D. Uplane, S.H. Pawar, Solid State Commun.46 (1983) 847.
- [8] D. Lue, P. Kamat, J. Phys. Chem. 97 (1993) 1073.

\*\*\*